ACCEPTED MANUSCRIPT
The Journal of Chemical Physics
AIP Publishing
This is the author's peer reviewed, accepted manuscript. However, the online version of record will be different from this version once it has been copyedited and typeset.
PLEASE CITE THIS ARTICLE AS DOI: 10.1063/5.0292162

Phenomenological determination of the isomerization transition state energy of carbonyl sulfide

Amine Rafik
Departamento de Ciencias Integradas y Centro de Estudios Avanzados en Física, Matemáticas y Computación, Universidad de Huelva, Huelva 21071, Spain and
Laboratory of Spectroscopy, Molecular Modeling, Materials, Nanomaterials, Water and Environment, LS3MN2E/CERNE2D, Faculty of Sciences, Mohammed V University in Rabat, Morocco
Jamil Khalouf-Rivera
Departamento de Ciencias Integradas y Centro de Estudios Avanzados en Física, Matemáticas y Computación, Universidad de Huelva, Huelva 21071, Spain
Francisco Pérez-Bernal
Departamento de Ciencias Integradas y Centro de Estudios Avanzados en Física, Matemáticas y Computación, Unidad Asociada GIFMAN, CSIC-UHU, Universidad de Huelva, Huelva 21071, Spain[a)]
Khadija Marakchi
Laboratory of Spectroscopy, Molecular Modeling, Materials, Nanomaterials, Water and Environment, LS3MN2E/CERNE2D, Faculty of Sciences, Mohammed V University in Rabat, Morocco
Miguel Carvajal
Departamento de Ciencias Integradas y Centro de Estudios Avanzados en Física, Matemáticas y Computación, Unidad Asociada GIFMAN, CSIC-UHU, Universidad de Huelva, Huelva 21071, Spain[a)]

(*Electronic mail: miguel.carvajal@dfa.uhu.es)

(Dated: 9 October 2025)

Signatures of excited-state quantum phase transitions in the bending degree of freedom of triatomic systems that undergo an isomerization reaction have been recently evinced. In this work, we study the carbonyl sulfide bending motion using an effective Hamiltonian within the two-dimensional limit of the vibron model framework, which has been shown to accurately describe critical phenomena in molecular bending spectra within experimental precision. To estimate the transition state energy barrier, we propose an improvement to a phenomenological formula proposed by Baraban *et al.* [1], introducing a new term to capture the anharmonicity change that characterizes quasilinear molecules.

I. INTRODUCTION

Transition State (TS) theory is a cornerstone in the study of chemical reactions, in particular, to determine reaction rates[2,3]. TS stands for a labile state at the top of the energy barrier, in-between the reactants and the products of a reaction process. Nevertheless, despite its relevance, TS properties are chiefly calculated using *ab initio* methods at different levels of theory, due to the lack of experimental information[4].

For isomerization reactions, a phenomenological formalism to determine the TS energy, based on the appearance of a dip in the energy gap of vibrational bending states excited along the reaction coordinate, has been recently developed[1,5]. However, the application of this approach is dependent on the availability of data for highly-excited levels, approaching the TS energy, in the bending vibrational band linked to the isomerization mechanism. This is a serious hindrance that can be overcome making use of accurate theoretical bending energy predictions, computed either *ab initio* or using an effective Hamiltonian. For instance, this approach has been successfully applied to determine the barrier height of the HCN-HNC isomerization reaction optimizing an effective algebraic Hamiltonian to reproduce spectroscopically assigned *ab initio* bending energies[6]. Despite the TS importance, the isomerization energy barrier for many simple systems remains unknown or insufficiently investigated. Nevertheless, this is not the case for carbonyl sulphide (OCS), whose isomerization barrier has been computed with *ab initio* methods[7] giving us results from a different approach to compare with and assess the quality of our results.

Carbonyl sulfide is a quasilinear molecule that has been spectroscopically characterized in the IR region, involving rovibrational energies up to $15\,000\,\mathrm{cm}^{-1}$ with vibrational angular momenta $\ell = 0 - 7$[8–17]. In recent years, this molecular species has gained a lot of attention due to its presence in Earth's atmosphere as well as in astronomical sources. Carbonyl sulfide is one of the most abundant sulfur-containing gases in the atmosphere, it has a relatively long chemical lifetime and contributes to the greenhouse effect with a significant warming potential[18]. This molecular species plays an important role in the formation of stratospheric sulfur aerosols and it is a possible probe for climate change due to its correlation with the biospheric uptake of CO_2[18,19]. In addition, it can be used as a tracer of biogenic activity and photosynthesis[20,21]. In astronomical sources, OCS has been observed in a variety of systems such as planetary atmospheres, the interstellar medium, and galaxies[22–25].

As regards the OCS vibrational structure, a number of theoretical studies can be found in the literature providing results for the rovibrational structure of OCS with spectroscopic accuracy. Variational calculations fitted the potential energy

[a)]Also at Instituto Carlos I de Física Teórica y Computacional, Universidad de Granada, Fuentenueva s/n, 18071 Granada, Spain

ACCEPTED MANUSCRIPT
The Journal of Chemical Physics
AIP Publishing
This is the author's peer reviewed, accepted manuscript. However, the online version of record will be different from this version once it has been copyedited and typeset.
PLEASE CITE THIS ARTICLE AS DOI: 10.1063/5.0292162

surface to the experimental energies using, e.g., different types of generalized internal coordinates[26], a self-consistent field-configuration interaction optimization method[27], algebraic techniques for the analytical determination of the matrix elements[28], and a polyad-conserving local algebraic model based on anharmonic ladder operators[29]. Empirical rovibrational levels were determined using MARVEL from the compilation of experimental transitions[30]. *Ab initio* methods were also applied to reproduce the energy levels and the transition lines based on higher-level calculations of the potential surface, refined empirically in some cases, and the dipole moment surface[31–34]. Up to our knowledge, there is only one study devoted to the computational modeling of the isomerization reaction of OCS[7]. In this work, the authors calculated the potential surface of the ground state simulating the isomerization reactions of the isomers of OCS, mainly at the CCSD(T)/aug-cc-pVTZ level of theory. The employed statistical methods allowed for estimating the barrier height for the isomerization of OCS. The authors found that the reaction barrier from the linear OCS to its linear COS isomer goes through a stable intermediate cyclic structure Δ-OCS. Despite the large number of works that have investigated the vibrational spectrum of OCS, the available levels lie well below halfway the estimated isomerization energy barrier.

In the present work we make use of the vibron model, a computationally efficient phenomenologic approach for the calculation of vibrational and rovibrational molecular spectra based on Lie algebras[35], that models molecular structure through collective bosonic excitations (vibrons)[36–39]. Different algebraic approaches, grounded on the original vibron model, were developed to avoid the mathematical complexity of the full rovibrational analysis in polyatomic molecules. In particular, we make use of the two-dimensional limit of the vibron model (2DVM), introduced to model vibrational bending degrees of freedom[39–41]. Despite its apparent simplicity, the 2DVM has been proven effective for describing not only the rigidly-linear and rigidly-bent limiting cases, but also the more involved quasilinear or non-rigid molecular spectra [41–43].

In the seminal work of Dixon [44], it was shown that the crossing of the barrier to linearity is evinced in the spectrum by a change in the pattern of energy spacings and the appearance of what was dubbed a *Dixon dip*. Numerous studies have subsequently explored the energy spectrum of nonrigid bent molecules, characterized by large amplitude vibrational degrees of freedom and capable of undergoing a bent-to-linear transition. These include, for instance, investigations into quasilinearity through the definition of a quantity to determine to what degree molecules are linear or bent[45], or introducing quantum monodromy to explain the dependence of energies with vibrational angular momentum and the absence of a set of vibrational quantum numbers globally valid for the entire spectrum[46,47].

Using a simplified 2DVM Hamiltonian, with a single control parameter, one can drive a bending degree of freedom of a molecular system from a rigidly-linear configuration to a rigidly-bent one[41]. At a critical value of the control parameter, the ground state of the system abruptly changes from a linear to a bent configuration. This is where the 2DVM ground-state quantum phase transition (GSQPT) occurs[41]. This phenomenology was extended to the realm of excited states[48–50]. For a given control parameter value, excited states may undergo a sudden change in their character when the excitation energy cross a critical energy threshold. Such transitions were named excited-state quantum phase transitions (ESQPTs), and can be accessed either by changing the control parameter for energies above the ground state energy or by increasing the energy for a constant control parameter value[41]. The ESQPT in the 2DVM was associated with the crossing of the barrier to linearity in nonrigid molecular systems. In fact, molecular bending spectra were the first systems where ESQPT precursors were identified in experimental setups and a set of characteristic spectral signatures were explained in a unified framework within the 2DVM[41,51–54]. Afterwards, it was found that, explicitly including anharmonicity in the 2DVM model Hamiltonian, an ESQPT appears that can be used to model isomerization processes[55]. In particular, the isomerization barrier height for the HCN-HNC system was obtained from the 2DVM results, identifying the ESQPT critical energy with the energy of the isomerization reaction transition state[6]. Recently, the 2DVM has also been used to measure the quantum chaoticity of a system using asymptotic values of an out-of-time-ordered correlator[56].

In the present work, we calculate the bending spectrum of the OCS molecule using the 2DVM, optimizing the parameters of a four-body algebraic Hamiltonian with existing experimental data, as has been done for other molecular species[53]. With the resulting energies and wave functions, we have studied the OCS bending spectrum, paying special heed to the vicinities of the ESQPT critical energy. To that end, quantities such as the participation ratio, the expectation value of the 2DVM number operator, the quasilinearity parameter, and the effective frequency are discussed. Concerning the effective frequency, we also propose a new empirical formula, based on the one presented in Ref.[1], which reproduces the anharmonicity trend observed in quasilinear molecules. Subsequently, making use of this formula, we estimate the barrier height associated with the isomerization of the OCS species.

II. THEORETICAL FRAMEWORK

A. The two dimensional limit of the vibron model

The 2DVM model, that stems from the vibron model[36], describes single (or coupled) molecular vibrational bending modes with one (or several copies of a) $U(3)$ dynamical algebra[40]. This model has been been applied to the study of the bending spectrum of various molecular systems[42,43,51–54,57–62]. Most notably, the model was shown to be capable of capturing the signatures of ground- and excited-state quantum phase transitions associated with the large-amplitude motion that occurs in bent-to-linear transitions[41,51–53]. As this model has been meticulously described before (see, e.g.,[41,53]), in the present work we only sketch the effective 2DVM Hamiltonian and the basis set used to charac-

ACCEPTED MANUSCRIPT
The Journal of Chemical Physics
AIP Publishing
This is the author's peer reviewed, accepted manuscript. However, the online version of record will be different from this version once it has been copyedited and typeset.
PLEASE CITE THIS ARTICLE AS DOI: 10.1063/5.0292162

terize the bending spectrum of the OCS molecular species.

There are two exactly-solvable limits under the 2DVM theoretical framework that correspond to rigid linear and bent configurations, respectively. The rigid linear case is associated mathematically with a truncated cylindrical harmonic oscillator (the $U(3) \supset U(2)$ dynamical symmetry) and the rigid bent case can be mapped to a 2D Morse oscillator (the $U(3) \supset SO(3)$ dynamical symmetry)[41]. Both subalgebra chains contain a common $SO(2)$ subalgebra with an associated quantum label, ℓ, that is the vibrational angular momentum in the linear case and the projection along the figure-axis of the rotational angular momentum in a rigid bent molecule. Each dynamical symmetry provides a possible basis set for performing the calculations. Due to the quasilinear nature of OCS, its equilibrium structure is linear and we use in our calculations the cylindrical oscillator basis. The quantum number N, which labels the totally-symmetric representation of $U(3)$ that spans the Hilbert space where calculations are carried out, is related to the total number of bound states of the system. States in the rigid linear case are denoted as $|[N];n\,\ell\rangle \equiv |n^{\ell}\rangle$. The quantum number n, that is the corresponding $U(2)$ Lie algebra irrep label, indicates the number of quanta of excitation of the 2D cylindrical oscillator and, as mentioned above, ℓ, is the system vibrational angular momentum. The branching rules for the cylindrical oscillator basis are given by

$$\begin{aligned} n &= N, N-1, N-2, ..., 0 \\ \ell &= \pm n, \pm(n-2), ..., \pm 1 \text{ or } 0 \text{ (n = odd or even)} . \end{aligned} \tag{1}$$

In this framework, we start with a general Hamiltonian including up to four-body interactions introduced in[53]. For OCS, after a careful selection of relevant operators, we have constructed an effective bending Hamiltonian that includes operators up to two-body interactions along with a three-body term

$$\hat{H} = P_1\hat{n} + P_2\hat{n}^2 + P_3\hat{\ell}^2 + P_4\hat{W}^2 + P_5\hat{n}\hat{\ell}^2 \,. \tag{2}$$

The interactions considered in this Hamiltonian can be constructed using the number operator, $\hat{n}$, which gives the number of quanta of excitation in the rigid linear limit, the vibrational angular momentum operator, $\hat{\ell}$, and the Casimir operator of the $SO(3)$ subalgebra, $\hat{W}^2$, which couples $|n^{\ell}\rangle$ with $|(n\pm 2)^{\ell}\rangle$ states. The $\hat{n}$ operator is cylindrical 2D Harmonic oscillator Hamiltonian and it is the zeroth-order description of a rigidly-linear molecule. The $\hat{W}^2$ operator models a one-dimensional anharmonic oscillator associated with the bending of a rigidly-bent molecule. A detailed study of both interactions can be found in[41]. When both interactions are combined, two different kind of states appear in the energy spectrum, separated by the ESQPT critical energy: in the higher end of the spectrum, states with positive anharmonicity and in the lower end states with negative anharmonicity. The transition from a non-linear to a linear configuration occurs at the critical energy. OCS being a linear molecule we include the $\hat{n}$ operator, together with an anharmonic correction provided by the $\hat{n}^2$ operator. The interplay between these two operators and the $\hat{W}^2$ operator allows for the description of OCS positive anharmonicity at low energies and the occurrence of an ESQPT related to the isomerization reaction[55]. The $\hat{\ell}^2$ interaction introduces vibrational angular momentum at the lowest order. After a carefully reckoning the role of all possible interactions up to four-body order, we have also included the $\hat{n}\hat{\ell}^2$ interaction that was found to improve the description of similar molecules[53]. Further details on the physical interpretation of the 2DVM operators can be found in Refs.[41,53]. Despite its simplicity, the effective Hamiltonian (2) allows us to carry out calculations of the OCS molecular vibrational energy structure with uncertainties close to spectroscopic accuracy. It is block diagonal in ℓ, as the vibrational angular momentum is conserved[53].

B. Effective frequency and isomerization transition energy

It should be highlighted that the 2DVM, although deceptively simple, possesses significant predictive power making it possible to compute highly excited states with good accuracy[51–53,63,64]. In fact, predicted bending term values at high energies were used to estimate the transition energy barrier between the HCN/HNC isomers[6] using a method presented previously by Baraban *et al.*[1]. Specifically, Baraban *et al.*[1] proposed a phenomenological formula for the effective frequency, ω^{eff}, as a function of the midpoint energies, $\bar{E}$, the mean value of adjacent vibrational energy levels, to determine the transition state.

$$\omega^{\text{eff}}(\bar{E}) = \omega_0 \left(1 - \frac{\bar{E}}{E_{\text{TS}}}\right)^{1/m_1} . \tag{3}$$

The midpoint energies $\bar{E}$ are obtained from the predicted bending spectrum, and the three parameters of the formula, ω_0, E_{TS}, and m_1, are optimized to fit $\bar{E}$ values. The ω_0 parameter is the fundamental frequency (ω^{eff} at $\bar{E}=0$), E_{TS} is the transition state energy, and m_1 is a parameter greater or equal than 2 which depends on the potential shape.

Eq. (3) can be applied to systems that range from a harmonic spectrum (constant $\omega^{\text{eff}} = \omega_0$, $m_1 \to \infty$) to a negative anharmonicity spectrum ($m_1 > 2$). However, quasilinear molecules, whose anharmonicity switches sign from positive to negative values, remain out of the scope of this formula. To encompass quasilinear cases, we propose a new formula, adding an extra term to Eq. (3)

$$\omega^{\text{eff}}(\bar{E}) = \omega_0 \left(1 - \frac{\bar{E}}{E_{TS}}\right)^{\frac{1}{m_1}} \left(1 + \frac{\bar{E}}{E_{TS}}\right)^{\frac{1}{m_2}} . \tag{4}$$

The proposed formula has four free parameters: ω_0, E_{TS}, m_1, and m_2. Eq. (3) is recovered from Eq. (4) when $m_2 \to \infty$. As in the Eq. (3) case, the new formula only describes states under the transition state energy, that implies a positive second factor. When the mid-point energy is close to zero, the first-order term of the Taylor expansion of Eq. (4) predicts an energy dependence in ω_0 units of $(1-x)^{\frac{1}{m_1}}(1+x)^{\frac{1}{m_2}} \approx 1 + \frac{m_1-m_2}{m_1 m_2}x + \mathcal{O}\left(x^2\right)$, where $x = \bar{E}/E_{TS}$. Hence, assuming a positive anharmonicity at low energies, the inequality $m_1 > m_2$ must be satisfied.

The zero point vibrational energy (ZPVE) of a quasilinear system can be estimated following the approach presented

ACCEPTED MANUSCRIPT
The Journal of Chemical Physics
AIP Publishing
This is the author's peer reviewed, accepted manuscript. However, the online version of record will be different from this version once it has been copyedited and typeset.
PLEASE CITE THIS ARTICLE AS DOI: 10.1063/5.0292162

in Baraban *et al.* [1] and using the modified formula Eq. (4). Once we have a continuous function that describes the midpoint energy as a function of the effective frequency, i.e., $\overline{E}(n) = \omega^{\text{eff}}\left(n+\frac{f}{2}\right)$, the ZPVE can be estimated solving numerically the integral

$$\int_0^{\text{ZPVE}} \frac{d\overline{E}}{\omega^{\text{eff}}(\overline{E})} = \frac{f}{2}\,, \tag{5}$$

where f is the number of vibrational degrees of freedom of the system. In particular, $f = 2$ for degenerate bending modes. In App. A, we solve Eq. (5) for the effective frequency formula given in Eq. (4).

III. RESULTS AND DISCUSSION

As already shown in Ref.[6], isomerization reaction barriers can be linked to the occurrence of an ESQPT in the bending degrees of freedom. Therefore, to determine the isomerization transition state energy, we can make use of quantities that are often used to characterize ESQPTs, such as the participation ratio (PR)[6,53–55,65,66], the expectation value of the number operator $(\hat{n})$[55,67], the quasilinearity parameter[53,55], or the effective frequency[1,5,53,55]. Thus, having the aim of determining the isomerization reaction barrier of OCS, we proceed to calculate the pure bending energies and wavefunctions.

To our knowledge, the available experimental dataset for bending vibrational levels of the main OCS isotopologue only includes states with vibrational angular momentum $\ell = 0,\ldots,7$ [8–15,17]. From this comprehensive data set, 71 term values are pure bending states. Out of these, 51 of them are experimental, with energies up to 8000 cm^{-1} [9,10,17], while the remaining 20 term values are predictions from a global analysis making use of an effective Hamiltonian, with energies up to 11 000 cm^{-1}[17]. The characterization of the bending spectrum is carried out in this work with the effective 2DVM Hamiltonian in Eq. (2), fitting its free parameters to the available data. We fit the P_i free parameters considering different values of N. We manually select the value of N that minimizes the deviation between calculated and both experimental and predicted data sets. A Python code was developed to calculate the energy levels and the free parameters are optimized using the nonlinear least squares minimization procedure provided by `lmfit` Python library[68]. The code is available upon request from the authors. The quality of the fit is assessed with the *rms*

$$rms = \sqrt{\frac{\sum_{k=1}^{N_{\text{data}}}\left(E_k^{\text{calc}} - E_k^{\text{exp}}\right)^2}{N_{\text{data}} - n_{\text{p}}}} \tag{6}$$

where E^{calc} are the calculated energies, E^{exp} are the experimental energies, N_{data} is the number of experimental energies, and n_p is the number of free parameters considered in the fitting procedure. In the OCS case, the 2DVM Hamiltonian $\hat{H}$ has five free parameters associated with all one- and two-body interactions plus a particular 3-body interaction.

TABLE I. Optimized Hamiltonian parameters for *Fit I* and *Fit II*, *rms* values (see main text), and number of term values included in the fit (N_{data}). All calculations were performed for a vibron number $N = 172$. Parameters' uncertainties are given in parentheses in units of the last quoted digits. Except N_{data}, all parameters and rms values are expressed in cm^{-1} units.

	Fit I	Fit II
P_1	2321.900(21)	2190.543(14)
P_2	-12.41738(12)	-11.58027(10)
P_3	4.3344(83)	3.9966(75)
P_4	-3.217143(46)	-3.015298(35)
P_5	0.00709(33)	0.007085(27)
N_{data}	51	71
$rms(fit)$	0.290	0.394
$rms(pred)$	1.550	0.430

We carried out two fits, dubbed *Fit I* and *Fit II*, with a vibron number $N = 172$. In *Fit I*, the parameters are optimized taking into consideration exclusively the 51 experimental bending term values. The obtained parameter values and their uncertainties are provided in the first column of Tab. I. In this case the *rms* is labeled as $rms(fit) = 0.29\,\text{cm}^{-1}$. If we include in the calculation the additional 20 term values obtained with an effective Hamiltonian, without further optimization, the result is $rms(pred) = 1.55\,\text{cm}^{-1}$, making clear that the predicted term values are in a reasonable agreement with the computed energy values. In fact, Yang and Noda [12] already showed that an effective Hamiltonian applied for characterizing the low vibrational levels of OCS can predict higher excited states within experimental accuracy. *Fit II* calculation includes in the fit both experimental and predicted term values, expanding the energy range of the fit to 11 000 cm^{-1}. The obtained results are given in the second column of Tab. I, with an $rms(fit) = 0.39\,\text{cm}^{-1}$, which lies very close to the expected experimental uncertainty. In this case, $rms(pred) = 0.43\,\text{cm}^{-1}$ is the *rms* obtained considering only the experimental term values and fixing the parameters to the optimized values of *Fit II*, obtaining a fit quality that is close enough to the results obtained in *Fit I*. The energies obtained in both fits, as well as the level assignment using rigid linear quantum numbers, and the residuals with experimental and predicted (marked with an asterisk) levels is provided in Tab. II. Calculated energy levels up to 16 000 cm^{-1} for the two reported fits are provided as supplementary data.

In order to compare the results obtained from *Fit I* and *Fit II*, we depict the residuals, i.e., the differences between the experimental and computed energies, in cm^{-1} units in Fig. 1. *Fit I* residuals for the 51 experimental term values are depicted using purple circles and the residuals for the 20 additional levels provided in Ref.[17] are depicted with red triangles. The relative residuals obtained with *Fit I* parameters for the states in the expanded dataset that lies in the range 8000 cm^{-1} to 11 000 cm^{-1} are below 0.05 %, with a largest residual $\Delta E = E^{\text{exp}} - E^{\text{cal}}$ of about 5 cm^{-1}. Finally, the relative residuals from *Fit II* are depicted with green crosses. In all cases, the accuracy is below 0.12 %.

Following the approach of Refs.[1,6], we use the calculated

ACCEPTED MANUSCRIPT
The Journal of Chemical Physics
AIP Publishing
This is the author's peer reviewed, accepted manuscript. However, the online version of record will be different from this version once it has been copyedited and typeset.
PLEASE CITE THIS ARTICLE AS DOI: 10.1063/5.0292162

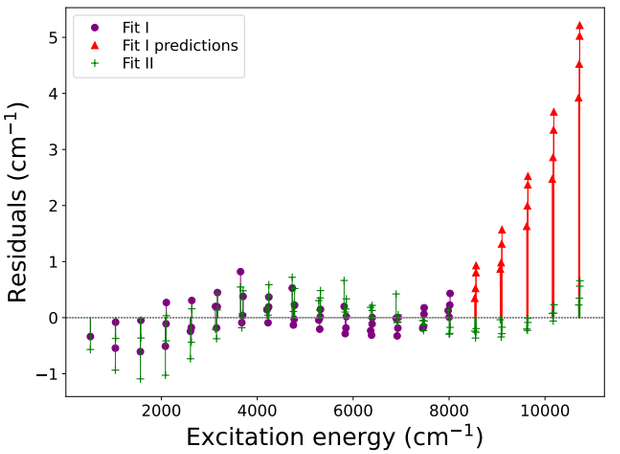

FIG. 1. Residuals for *Fit I* and *Fit II* calculations versus the experimental and predicted energies in cm^{-1} units. Purple circles show the residuals obtained from *Fit I* for 51 experimental energies. Red triangles include the predictions of *Fit I* for the 20 term values in the energy range from 8000 cm^{-1} to 11 000 cm^{-1} obtained with an effective Hamiltonian[17]. Green crosses correspond to the residuals for *Fit II*, including 71 experimental and predicted bending term values.

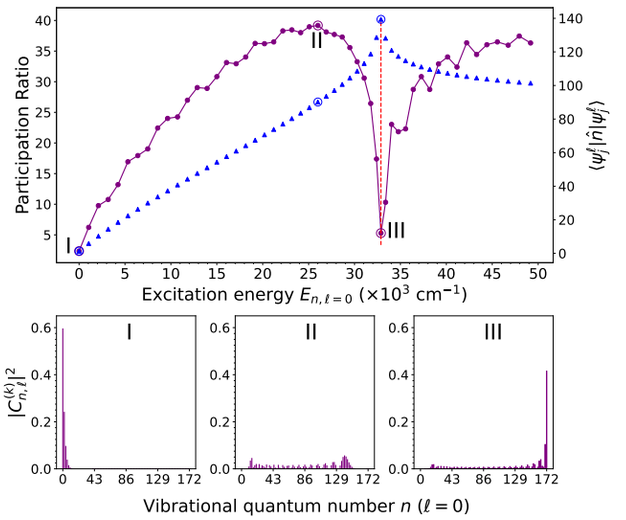

FIG. 2. Upper panel: Participation ratio (purple dots) and expectation value of the $\hat{n}$ operator (blue triangles) as a function of the computed bending term values for $\ell = 0$ states obtained in *Fit I*. Lower panels: Squared components $|C_{n,\ell}^{(k)}|^2$ as a function of the vibrational quantum number n for $\ell = 0$ for three selected eigenstates (I, II, and III) marked in the upper panel with circles.

energies and wave functions to locate the critical energy of the ESQPT, which is our estimation of the transition state energy. We use different quantities that are convenient probes for the ESQPT. The first one is the PR, a quantity that measures the level of localization of wave functions in a given basis[69]. It was shown that the participation ratio when eigenstates are expressed in the basis associated with a particular dynamical symmetry is a convenient probe for the location of the ESQPT critical energy[65,66]. The participation ratio is defined as

$$PR\left(\left|\psi_k^\ell\right\rangle\right) = \frac{1}{\sum_n |C_{n,\ell}^{(k)}|^4}\,, \tag{7}$$

where $\left|\psi_k^\ell\right\rangle$ is an eigenstate with vibrational angular momentum ℓ. The eigenstates $\{\left|\psi_k^\ell\right\rangle\}$ can be expressed as $\left|\psi_k^\ell\right\rangle = \sum_{n=0} C_{n,\ell}^{(k)} \left|n\,\ell\right\rangle$. The lower the value of PR, the more localized is the state under study in the given basis set with a minimum value of unity if the eigenstate is a basis state. Conversely, the larger the value of the PR, the more spread out is the state, with a maximum value equal to the dimension of the ℓ angular momentum Hamiltonian block. A second hallmark of the ESQPT that allows us to localize the TS energy is revealed by the expectation value of the $\hat{n}$ operator, $\left\langle\psi_k^\ell\right|\hat{n}\left|\psi_k^\ell\right\rangle$, which is the operator used as an order parameter for the second-order ground-state quantum phase transition[41]. We depict in Fig. 2 the PR and the expectation value of $\hat{n}$ for the $\ell = 0$ eigenfunctions obtained in *Fit I* as a function of the calculated term values in cm^{-1} units. The purple line is the PR and the blue triangles mark the expectation value of $\hat{n}$. The PR results in Fig. 2 indicate that, as expected, eigenstates are more delocalized in the basis as the energy increases from the ground state. This is followed by a striking decrease to a minimum PR value, observed around 33 000 cm^{-1}, that marks the ESQPT critical energy[53,65,66] which in this case is associated with the isomerization reaction transition state energy[6]. Three eigenstates of OCS with $\ell = 0$, designated as I, II, and III, have been chosen to examine the eigenstate structure at different excitation energies. In particular, eigenstate I is the ground state, eigenstate II lies at an energy halfway between the energy of states I and III, and eigenstate III is the eigenstate with a minimum PR value. The squared wave function components, $|C_{n,\ell}^{(k)}|^2$, of these three eigenstates as a function of the quantum number n in the $|n\,\ell\rangle$ basis are shown as bar plots in the three lower panels of Fig. 2. The bar plots indicate that eigenstates I and III are significantly localized while eigenstate II is delocalized in the states of the basis set, confirming the PR results. Wavefunction I has a squared component around 0.6 in the basis state $|n = 0\,, \ell = 0\rangle$ and wavefunction III is localized in the last basis state, $|n = N\,, \ell = 0\rangle$, of the basis set with a squared component close to 0.4. The minimum PR value is linked to the existence of an ESQPT, which is in fact connected to anharmonicity effects in the Hamiltonian[55,67] and associated with the isomerization transition in the system[6]. Regarding the expectation value of the number operator, $\hat{n}$, as a probe for the system's isomerization, this is evaluated for the different system eigenstates. This quantity is depicted in Fig. 2 as a function of the excitation energy, and its maximum value is located at the ESQPT critical energy, a result that agrees with the PR result. The red dashed vertical line indicates the isomerization TS energy obtained with the modified empirical formula proposed for the effective frequency $\omega^{\rm eff}$ in Eq. (4). The PR and expected values of $\hat{n}$ for the eigenfunctions of *Fit II* are reported in the supplementary material.

Another quantity of interest in the case of molecular bend-

ACCEPTED MANUSCRIPT
The Journal of Chemical Physics
AIP Publishing
This is the author's peer reviewed, accepted manuscript. However, the online version of record will be different from this version once it has been copyedited and typeset.
PLEASE CITE THIS ARTICLE AS DOI: 10.1063/5.0292162

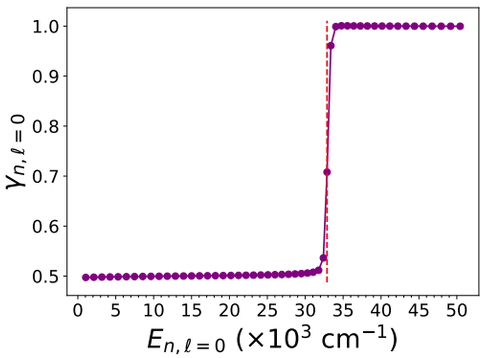

FIG. 3. Quasilinearity parameter $\gamma_{n,\ell=0}$ as a function of the bending energies calculated using the Hamiltonian (2) in *Fit I*.

ing vibrations is the quasilinearity parameter

$$\gamma_{n,\ell} = \frac{E_{n+1,\ell+1} - E_{n,\ell}}{E_{n+2,\ell} - E_{n,\ell}} \quad , \tag{8}$$

originally proposed by Yamada and Winnewisser[45] to examine the degree of quasilinearity of the molecular bending modes and recently extended to the study of ESQPTs in the bending vibration of molecules[55]. In this framework, the quasilinearity parameter is equal to 0.5 for the bending mode of a rigidly-linear molecule with symmetry $\mathscr{C}_{\infty v}$ or $\mathscr{D}_{\infty h}$. In the OCS case, the $\gamma_{n,0}$ parameter as a function of the excitation bending energies for *Fit I* results is shown in Fig. 3. The value of $\gamma_{n,0} = 0.5$ for the OCS ground and lowest excited states clearly indicate that this molecular species can be considered a linear molecule within this energy range. A sudden rise of the value of $\gamma_{n,0}$ to a value of 1 occurs in the region of 33 000 cm^{-1}, at the ESQPT critical energy[55]. We associate this OCS structural change with the isomerization transition state energy, a result that is consistent with the isomerization energy barrier value estimated with the PR and the expectation value of the number operator.

From the results obtained for the PR, the expected value of $\hat{n}$, and the quasilinearity parameter, we have a broad estimation of the transition state energy in the range 33 000 cm^{-1}. Nevertheless, a more precise estimate can be obtained based on the variation of the effective frequency ω^{eff}, computed from the 2DVM predictions for the bending energies of OCS. In Fig. 4, we plot the values of ω^{eff} obtained from the 2DVM predictions with $\ell = 0$ of *Fit I* (black circles) as a function of the midpoint bending energies. We have also included the available experimental data, lying in the energy range 0 cm^{-1} to 8000 cm^{-1} (green triangles), and the extended data with $\ell = 0$, found in the 8000 cm^{-1} to 11 000 cm^{-1} energy range (blue squares). We would like to emphasize that the values of ω^{eff} predicted from the spectrum of *Fit I* plunge as the excitation energy approaches the expected isomerization barrier energy, providing an estimate of this critical parameter.

A finer estimate of the isomerization barrier of OCS can be determined using a phenomenological approach, as proposed by Baraban *et al.*[1]. This approach allows us to determine the TS energy more accurately by fitting the ω_0, E_{TS}, and m_1 parameters in the phenomenological formula (3) to optimize the agreement with the computed effective frequency values. The purple line in Fig. 4 corresponds to the results of this fit (3), which provides a reasonable description of the effective frequency dip.

However, improved results can be obtained from the extended equation (4). The fit of this formula to the midpoint energies predicted by *Fit I* is shown as an orange line in Fig. 4. Comparing the results obtained with both phenomenological equations, it is clear that, at the cost of including the new parameter m_2, the results obtained with Eq. (4) have a better agreement with effective frequency values at low energies. Hence, the new empirical formula Eq. (4) corrects the trend of the effective frequency for molecules with quasilinear character.

A summary of the results obtained in the present work for the OCS TS energy and ZPVE, as well as the values in the literature obtained with *ab initio* calculations can be found in Table III. The values of E_{TS} and ZPVE from *ab initio* calculations were calculated at a CCSD(T)/aug-cc-pVTZ level using `Gaussian G09` and `CFOUR`[7]. Two values for the TS energy of the reaction OCS $\rightarrow \Delta-$OCS were calculated. The TS energy was calculated at 33052 cm^{-1} using `Gaussian09`, and at 33611 cm^{-1} with `CFOUR`. The difference of 559 cm^{-1} may be attributed to possible different algorithms or basis set implementations in the two codes. In addition, the two codes have a different set of defaults, in particular, `Gaussian09` uses the frozen core approximation. As regards our results, we provide the results obtained optimizing the parameters in effective frequency formulas in Eqs. (3) and (4) to the 2DVM bending energy predictions from *Fit I* and *Fit II*. The values E_{TS} from *Fit I* results and Eqs. (3) and (4) are 33240 and 33409 cm^{-1}, respectively. The results obtained considering *Fit II* data are 35769 and 36005 cm^{-1}. The barrier to OCS isomerization determined by this procedure is in good agreement with the *ab initio* results estimated at 33052/33611 cm^{-1} using G09 and CFOUR[7]. The differences of the E_{TS} value obtained for OCS with *Fit I* and *Fit II* compared to *ab initio* G09 and CFOUR calculations are 0.6% and 1.1%, and 8.2% and 6.4% respectively for Eq. (3), and 1.1% and 0.6%, and 8.9% and 7.1% respectively for Eq. (4). Therefore, it can be highlighted that the combination of the computationally inexpensive 2DVM approach, with phenomenological formulas (3) and (4), can provide a reasonable estimation of the isomerization barrier of OCS, in line with results calculated with the golden standard method CCSD(T). As regards the ZPVE estimation, the results obtained with Eq. (4), using *Fit I* and *Fit II* results, are notably closer to the known estimates than the results obtained using Eq. (3) from Ref.[1]. The maximum deviation of ZPVE in both fits with respect to the *ab initio* bending fundamental is about 8.7% using Eq. (3) and 2.2% for Eq. (4). In addition, the ancillary optimized parameters ω_0, m_1 and m_2 are also provided in Table III.

Thus, considering the TS results obtained for the OCS molecule, we can conclude that the optimization of Eq. (4) parameters to match the 2DVM predictions provides an accurate estimation of the isomerization transition state energy,

ACCEPTED MANUSCRIPT
The Journal of Chemical Physics
AIP Publishing
This is the author's peer reviewed, accepted manuscript. However, the online version of record will be different from this version once it has been copyedited and typeset.
PLEASE CITE THIS ARTICLE AS DOI: 10.1063/5.0292162

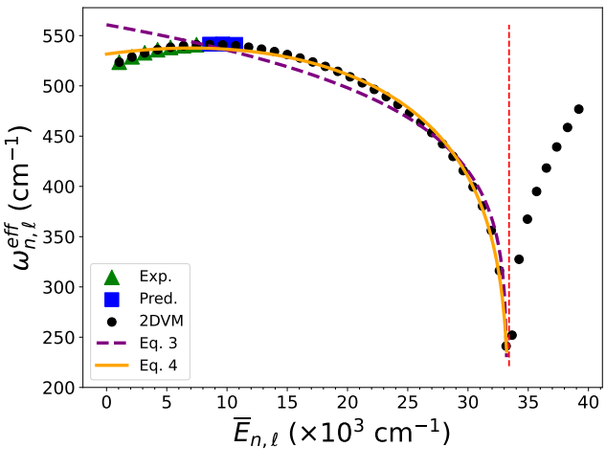

FIG. 4. Effective frequency as a function of the midpoint bending energy for $\ell = 0$ states computed for *Fit I* results. Green triangles and blue squares are the available experimental and extended energy data. Black circles are the 2DVM results. Purple and orange lines are obtained fitting Eqs. (3) and (4) to *Fit I* results, respectively.

even when the available levels lie well below half the estimated isomerization energy barrier.

IV. CONCLUSIONS

The bending spectrum of the OCS molecule is calculated within experimental accuracy using the 2DVM approach. Despite the lack of experimental data for highly-excited bending levels, this algebraic model successfully predicts the spectrum with sufficient accuracy to estimate the isomerization barrier, yielding results comparable to those obtained from *ab initio* methods. The spectroscopic signatures of the TS in OCS have been characterized by several quantities: the participation ratio, the expectation value of the $\hat{n}$ operator, the quasilinearity parameter, and the effective frequency. The agreement between these indicators and *ab initio* computed TS properties highlights the quality of the bending energies and wavefunctions obtained using the 2DVM approach.

Furthermore, the isomerization barrier height estimated using the semiempirical formula developed by Baraban *et al.* [1] aligns well with *ab initio* results. However, this formula does not adequately capture the tendency of quasilinear molecules to exhibit a sign change in anharmonicity—from positive to negative— as the energy approaches the linearity barrier. In the case of OCS, this change is observed at $v_b = (n-|\ell|)/2 = 7$, where the slope of the effective frequency reverses. To address this, we propose a new phenomenological formula for the effective frequency [Eq. (4)], which better accounts for the anharmonic behavior at low vibrational states. This improved formula yields a more accurate fit to the effective frequencies and provides an isomerization barrier height in very good agreement with the *ab initio* golden standard.

Considering the promising results obtained for the carbonyl sulfide bending spectrum and its transition state energy, our next step will be to present an algebraic model that includes all vibrational degrees of freedom (see, e.g., Ref.[61,62]) in order to delve deeper into the interactions between stretching and bending vibrational states and how this interaction influence of the isomerization barrier height.

ACKNOWLEDGMENTS

This research has received funding from the European Union's Horizon 2020 research and innovation program under the Marie Skodowska-Curie Grant Agreement No. 872081 and Grant No. PID2022-136228NB-C21 funded by MICIU/AEI/10.13039/501100011033 and, as appropriate, by "ERDF A way of making Europe, by ERDF/EU," by the European Union, or by the European Union NextGenerationEU/PRTR. This work was also partially supported by the Consejería de Universidad, Investigación e Innovación, Junta de Andalucía and European Regional Development Fund (ERDF 2021–2027) under the project EPIT1462023. Computing resources supporting this work were provided by the CEAFMC and Universidad de Huelva High Performance Computer located in the Campus Universitario "El Carmen" and funded by FEDER/MINECO Project No. UNHU-15CE-2848.

Appendix A: Zero point vibrational energy

To estimate the ZPVE we have followed the methodology presented by Baraban *et al.* [1]. The integral in Eq. (5), considering the effective frequency given by Eq. (3), is analytically solvable and, therefore, we can find an expression for the ZPVE (see the supplementary material of Ref.[1] for further information). However, we cannot provide an explicit formula when we consider the modified parametrization given by Eq. (4). In this case, the resulting integral is

ACCEPTED MANUSCRIPT
The Journal of Chemical Physics
AIP Publishing
This is the author's peer reviewed, accepted manuscript. However, the online version of record will be different from this version once it has been copyedited and typeset.
PLEASE CITE THIS ARTICLE AS DOI: 10.1063/5.0292162

TABLE II. Experimental ($E^{\rm exp}$) and computed bending energies ($E^{\rm cal}$) obtained from *Fit I* and *Fit II* expressed in $\rm cm^{-1}$ units. Residual values, $\Delta E = E^{\rm exp} - E^{\rm cal}$, are also provided.

(n,ℓ)	$E^{\rm expa}$	$E^{\rm cal}$(*Fit I*)	ΔE	$E^{\rm cal}$ (*Fit II*)	ΔE	(n,ℓ)	$E^{\rm expa}$	$E^{\rm cal}$(*Fit I*)	ΔE	$E^{\rm cal}$ (*Fit II*)	ΔE
(0, 0)	0.0	0.0	0.0	0.0	0.0	(13, 3)	6931.30[17]	6931.48	-0.19	6931.37	-0.08
(2, 0)	1047.04[9]	1047.12	-0.08	1047.41	-0.37	(15, 3)	8014.46[17]	8014.23	0.22	8014.74	-0.28
(4, 0)	2104.83[9]	2104.56	0.27	2104.79	0.04	*(17, 3)	9098.23[17]	9096.91	1.32	9098.51	-0.29
(6, 0)	3170.64[10]	3170.19	0.45	3170.21	0.44	*(19, 3)	10181.71[17]	10178.36	3.35	10181.63	0.08
(8, 0)	4242.55[10]	4242.18	0.37	4241.96	0.59	(4, 4)	2084.37[10]	2084.88	-0.51	2085.4	-1.03
(10, 0)	5319.01[17]	5318.87	0.15	5318.53	0.48	(6, 4)	3151.68[17]	3151.86	-0.18	3152.05	-0.38
(12, 0)	6398.75[17]	6398.75	0.0	6398.54	0.22	(8, 4)	4225.02[10]	4225.11	-0.09	4224.97	0.05
(14, 0)	7480.64[17]	7480.47	0.18	7480.71	-0.06	(10, 4)	5302.79[17]	5302.99	-0.21	5302.65	0.13
*(16, 0)	8563.67[17]	8562.74	0.93	8563.86	-0.2	(12, 4)	6383.71[17]	6384.02	-0.31	6383.72	-0.01
*(18, 0)	9646.90[17]	9644.38	2.52	9646.91	-0.01	(14, 4)	7466.67[17]	7466.83	-0.16	7466.9	-0.23
*(20, 0)	10729.45[17]	10724.24	5.21	10728.8	0.66	*(16, 4)	8550.67[17]	8550.15	0.52	8551.03	-0.36
(1, 1)	520.42 [9]	520.76	-0.34	520.99	-0.57	*(18, 4)	9634.79[17]	9632.8	2.0	9635.02	-0.23
(3, 1)	1573.37[9]	1573.41	-0.05	1573.73	-0.36	*(20, 4)	10718.17[17]	10713.64	4.52	10717.82	0.35
(5, 1)	2635.59[9]	2635.28	0.31	2635.43	0.16	(5, 5)	2606.57[17]	2606.82	-0.24	2607.3	-0.73
(7, 1)	3704.77[10]	3704.39	0.38	3704.29	0.48	(7, 5)	3677.79[17]	3677.88	-0.09	3677.97	-0.18
(9, 1)	4779.23[17]	4779.0	0.22	4778.7	0.52	(9, 5)	4754.19[17]	4754.33	-0.13	4754.08	0.11
(11, 1)	5857.56[17]	5857.54	0.02	5857.22	0.33	(11, 5)	5834.33[17]	5834.61	-0.29	5834.23	0.1
(13, 1)	6938.58[17]	6938.58	0.0	6938.53	0.05	(13, 5)	6916.99[17]	6917.32	-0.33	6917.08	-0.09
(15, 1)	8021.22[17]	8020.79	0.43	8021.4	-0.17	(15, 5)	8001.14[17]	8001.14	0.01	8001.44	-0.29
*(17, 1)	9104.52[17]	9102.95	1.57	9104.69	-0.17	*(17, 5)	9085.83[17]	9084.85	0.98	9086.17	-0.34
*(19, 1)	10187.57[17]	10183.9	3.67	10187.34	0.23	*(19, 5)	10170.15[17]	10167.29	2.86	10170.21	-0.06
(2, 2)	1041.29[9]	1041.84	-0.54	1042.23	-0.94	(6, 6)	3129.21[17]	3129.01	0.2	3129.42	-0.21
(4, 2)	2099.52[9]	2099.63	-0.11	2099.94	-0.41	(8, 6)	4203.97[17]	4203.83	0.14	4203.8	0.18
(6, 2)	3165.80[9]	3165.61	0.19	3165.66	0.14	(10, 6)	5283.16[17]	5283.2	-0.04	5282.86	0.3
(8, 2)	4238.10[10]	4237.91	0.19	4237.71	0.39	(12, 6)	6365.42[17]	6365.65	-0.23	6365.23	0.18
(10, 2)	5314.91[17]	5314.89	0.01	5314.56	0.35	(14, 6)	7449.63[17]	7449.82	-0.19	7449.68	-0.05
(12, 2)	6394.95[17]	6395.07	-0.11	6394.83	0.13	*(16, 6)	8534.79[17]	8534.45	0.35	8535.03	-0.24
(14, 2)	7477.12[17]	7477.06	0.06	7477.25	-0.13	*(18, 6)	9619.99[17]	9618.36	1.63	9620.19	-0.2
*(16, 2)	8560.39[17]	8559.59	0.8	8560.65	-0.26	*(20, 6)	10704.36[17]	10700.44	3.92	10704.13	0.23
*(18, 2)	9643.85[17]	9641.48	2.37	9643.93	-0.09	(7, 7)	3652.28[17]	3651.46	0.82	3651.73	0.55
*(20, 2)	10726.61[17]	10721.59	5.02	10726.05	0.56	(9, 7)	4730.27[17]	4729.74	0.53	4729.55	0.72
(3, 3)	1562.61[9]	1563.22	-0.61	1563.7	-1.09	(11, 7)	5811.96[17]	5811.76	0.2	5811.3	0.66
(5, 3)	2625.61[9]	2625.78	-0.18	2626.04	-0.44	(13, 7)	6896.12[17]	6896.13	-0.01	6895.7	0.42
(7, 3)	3695.58[10]	3695.54	0.04	3695.51	0.07	(15, 7)	7981.67[17]	7981.55	0.13	7981.54	0.13
(9, 3)	4770.74[17]	4770.77	-0.03	4770.49	0.25	*(17, 7)	9067.67[17]	9066.8	0.87	9067.7	-0.04
(11, 3)	5849.71[17]	5849.89	-0.18	5849.55	0.15	*(19, 7)	10153.21[17]	10150.74	2.47	10153.13	0.08

[a] As experimental data are considered those collected from Refs.[9,10] and the predictions in the range $0\,\rm cm^{-1}$ to $8000\,\rm cm^{-1}$ computed with an effective Hamiltonian from Ref.[17]. The predicted energies in the range $8000\,\rm cm^{-1}$ to $11\,000\,\rm cm^{-1}$[17] are marked with an asterisk. *Fit I* only considers the experimental data but compares their higher excited energy calculations with those marked with an asterisk. *Fit II* uses both the experimental and predicted term values marked with an asterisk.

TABLE III. Quantitative comparison of *ab initio* TS and ZPVE (in units of $\rm cm^{-1}$) and our results computed with the effective frequency formula from Ref.[1] and Eq. (4) using the 2DVM bending energy predictions from Fit I and Fit II. Uncertainties are given in parentheses in units of the last quoted digits.

Source	TS	ZPVE	ω_0	m_1	m_2
G09/CFOUR[a]	33052/33611	520.6/524.5	—	—	—
Fit I, Eq. (3)[b]	33240(24)	560.5(38)	560.8(38)	7.76(38)	—
Fit I, Eq. (4)	33409(37)	532.1(21)	531.6(21)	4.99(15)	3.28(22)
Fit II, Eq. (3)[a]	35769(44)	565.8(48)	566.2(49)	6.78(38)	—
Fit II, Eq. (4)	36005(65)	528.7(29)	528.1(30)	4.16(16)	2.52(19)

[a] *Ab initio* results calculated at CCSD(T)/aug-cc-pVTZ level of theory using Gaussian G09 and CFOUR[7]. ZPVE for the bending spectrum is estimated as the fundamental energy ω_b.

[b] The phenomenological formula from Ref.[1] given in Eq.(3)

ACCEPTED MANUSCRIPT
The Journal of Chemical Physics
AIP Publishing
This is the author's peer reviewed, accepted manuscript. However, the online version of record will be different from this version once it has been copyedited and typeset.
PLEASE CITE THIS ARTICLE AS DOI: 10.1063/5.0292162

$$\begin{aligned}\int_0^{\mathrm{ZPVE}} \frac{d\overline{E}}{\omega^{\mathrm{eff}}(\overline{E})} &= \frac{1}{\omega_0}\int_0^{\mathrm{ZPVE}} \left(1-\frac{\overline{E}}{E_{\mathrm{TS}}}\right)^{\frac{-1}{m_1}} \left(1+\frac{\overline{E}}{E_{\mathrm{TS}}}\right)^{\frac{-1}{m_2}} d\overline{E} \\ &= \frac{E_{\mathrm{TS}}}{2^{\frac{1}{m_1}}\,\omega_0}\,\frac{m_2}{(m_2-1)}\left[-{}_2F_1\left(\frac{1}{m_1},\frac{m_2-1}{m_2},\frac{2m_2-1}{m_2},\frac{1}{2}\right)\right. \\ &\quad \left. + \left(\frac{\mathrm{ZPVE}+E_{\mathrm{TS}}}{E_{\mathrm{TS}}}\right)^{\frac{m_2-1}{m_2}} {}_2F_1\left(\frac{1}{m_1},\frac{m_2-1}{m_2},\frac{2m_2-1}{m_2},\frac{\mathrm{ZPVE}+E_{\mathrm{TS}}}{2E_{\mathrm{TS}}}\right)\right] \\ &= \frac{f}{2}\,,\end{aligned} \tag{A1}$$

where ${}_2F_1\,(a,b,c,d)$ is the hypergeometric function and $f=2$ in the case of the degenerate bending modes.

The values of the unknown parameters are determined by an iterative minimization process. First, we estimate ω_0, E_{TS}, m_1, and m_2 in Eq. (4) without a zero point energy. Then, we solve numerically Eq. (A1) to determine a first approach to the ZPVE and, using this value, we shift the energies and repeat this process recursively until we reach the desired tolerance.

[1]J. H. Baraban, P. B. Changala, G. C. Mellau, J. F. Stanton, A. J. Merer, and R. W. Field, "Spectroscopic characterization of isomerization transition states," Science **350**, 1338–1342 (2015).
[2]H. Eyring and M. Polanyi, "On simple gas reactions," Z. Phys. Chem. B **12**, 279 (1931).
[3]M. J. Nye, "Working tools for theoretical chemistry: Polanyi, Eyring, and debates over the "semiempirical method"," J. Comput. Chem. **28**, 98–108 (2007).
[4]J. C. Polanyi and A. H. Zewail, "Direct observation of the transition state," Acc. Chem. Res. **28**, 119–132 (1995).
[5]G. C. Mellau, A. A. Kyuberis, O. L. Polyansky, N. Zobov, and R. W. Field, "Saddle point localization of molecular wavefunctions," Scientific Reports **6**, 33068 (2016).
[6]J. Khalouf-Rivera, M. Carvajal, L. F. Santos, and F. Pérez-Bernal, "Calculation of transition state energies in the HCN–HNC isomerization with an algebraic model," The Journal of Physical Chemistry A **123**, 9544–9551 (2019).
[7]G. A. Lara-Cruz and G. E. Moyano, "OCS isomerization and dissociation kinetics from statistical models," Theoretical Chemistry Accounts **137**, 79 (2018).
[8]A. G. Maki, E. K. Plyler, and E. D. Tidwell, "Vibration-rotation bands of carbonyl sulfide," Journal of Research of the National Bureau of Standards. Section A, Physics and Chemistry **66**, 163 (1962).
[9]A. Fayt, R. Vandenhaute, and J. G. Lahaye, "Global rovibrational analysis of carbonyl sulfide," Journal of Molecular Spectroscopy **119**, 233–266 (1986).
[10]A. Belafhal, A. Fayt, and G. Guelachvili, "Fourier Transform Spectroscopy of carbonyl sulfide from 1800 to 3120 cm^{-1}: The normal species," J. Mol. Spectroscopy **174**, 1–19 (1995).
[11]C. Hornberger, B. Boor, R. Stuber, W. Demtroder, S. Naïm, and A. Fayt, "Sensitive overtone spectroscopy of carbonyl sulfide between 6130 and 6650 cm^{-1} and at 12000 cm^{-1}," J. Mol. Spectroscopy **179**, 237–245 (1996).
[12]X. Yang and C. Noda, "Vibrational overtone transitions of OCS in the near infrared," Journal of Molecular Spectroscopy **183**, 151–156 (1997).
[13]E. Rbaihi, A. Belafhal, J. Vander Auwera, S. Naïm, and A. Fayt, "Fourier Transform Spectroscopy of carbonyl sulfide from 4800 to 8000 cm^{-1} and new global analysis of $^{16}\mathrm{O}^{12}\mathrm{C}^{32}\mathrm{S}$," Journal of Molecular Spectroscopy **191**, 32–44 (1998).
[14]S. Naïm, A. Fayt, H. Bredohl, J.-F. Blavier, and I. Dubois, "Fourier transform spectroscopy of carbonyl sulfide from 3700 to 4800 cm^{-1} and selection of a line-pointing program," J. Mol. Spectroscopy **192**, 91–101 (1998).
[15]B. Frech, M. Murtz, P. Palm, R. Lotze, W. Urban, and A. Maki, "Sub-Doppler Heterodyne frequency measurements on OCS near 2900 cm^{-1} using a co overtone sideband spectrometer," J. Mol. Spectroscopy **190**, 91–100 (1998).
[16]S. Tranchart, I. Hadj Bachir, T. Huet, A. Olafsson, J.-L. Destombes, S. Naı¨m, and A. Fayt, "High-resolution laser photoacoustic spectroscopy of ocs in the 12000–13000 cm^{-1} region," Journal of Molecular Spectroscopy **196**, 265–273 (1999).
[17]D. Golebiowski, X. de Ghellinck d'Elseghem Vaernewijck, M. Herman, J. Vander Auwera, and A. Fayt, "High sensitivity (femto-FT-CEAS) spectra of carbonyl sulphide between 6200 and 8200cm^{-1}, and new energy pattern in the global rovibrational analysis of $^{16}\mathrm{O}^{12}\mathrm{C}^{32}\mathrm{S}$," Journal of Quantitative Spectroscopy and Radiative Transfer **149**, 184–203 (2014).
[18]C. Brühl, J. Lelieveld, P. J. Crutzen, and H. Tost, "The role of carbonyl sulphide as a source of stratospheric sulphate aerosol and its impact on climate," Atmospheric Chemistry and Physics **12**, 1239–1253 (2012).
[19]J. Ma, L. M. J. Kooijmans, A. Cho, S. A. Montzka, N. Glatthor, J. R. Worden, L. Kuai, E. L. Atlas, and M. C. Krol, "Inverse modelling of carbonyl sulfide: implementation, evaluation and implications for the global budget," Atmospheric Chemistry and Physics **21**, 3507–3529 (2021).
[20]J. E. Campbell, G. R. Carmichael, T. Chai, M. Mena-Carrasco, Y. Tang, D. Blake, N. Blake, S. A. Vay, G. J. Collatz, I. Baker, *et al.*, "Photosynthetic control of atmospheric carbonyl sulfide during the growing season," Science **322**, 1085–1088 (2008).
[21]J. A. De Gouw, C. Warneke, S. A. Montzka, J. S. Holloway, D. D. Parrish, F. C. Fehsenfeld, E. L. Atlas, R. J. Weber, and F. M. Flocke, "Carbonyl sulfide as an inverse tracer for biogenic organic carbon in gas and aerosol phases," Geophysical research letters **36**, L05804 (2009).
[22]E. Lellouch, G. Paubert, R. Moreno, M. C. Festou, B. Bézard, D. Bockelée-Morvan, P. Colom, J. Crovisier, T. Encrenaz, D. Gautier, *et al.*, "Chemical and thermal response of jupiter's atmosphere following the impact of comet Shoemaker–Levy 9," Nature **373**, 592–595 (1995).
[23]B. Bézard, C. De Bergh, D. Crisp, and J.-p. Maillard, "The deep atmosphere of venus revealed by high-resolution nightside spectra," Nature **345**, 508–511 (1990).
[24]K. B. Jefferts, A. A. Penzias, R. W. Wilson, and P. M. Solomon, "Detection of interstellar carbonyl sulfide," Astrophysical Journal **168**, L111–L113 (1971).
[25]R. Mauersberger, C. Henkel, and Y.-N. Chin, "Dense gas in nearby galaxies. viii. the detection of OCS," Astronomy and Astrophysics **294**, 23–32 (1995).
[26]J. Zúñiga, A. Bastida, M. Alacid, and A. Requena, "Excited vibrational states and potential energy function for OCS determined using generalized internal coordinates," The Journal of Chemical Physics **113**, 5695–5704 (2000).
[27]D. Xie, Y. Lu, D. Xu, and G. Yan, "Theoretical studies on the potential energy surface and rovibrational states for the electronic ground state of carbonyl sulfide," Chemical Physics **270**, 415–428 (2001).
[28]T. Sedivcová-Uhlíková, H. Y. Abdullah, and N. Manini, "Algebraic-matrix calculation of vibrational levels of triatomic molecules," The Journal of

ACCEPTED MANUSCRIPT
The Journal of Chemical Physics
AIP Publishing
This is the author's peer reviewed, accepted manuscript. However, the online version of record will be different from this version once it has been copyedited and typeset.
PLEASE CITE THIS ARTICLE AS DOI: 10.1063/5.0292162

Physical Chemistry A **113**, 6142–6148 (2009).
[29]E. Suárez, O. Guzmán-Juárez, and R. Lemus, "Description of vibrational excitations of the OCS molecule using a local algebraic approach," J. Quant. Spectr. Rad. Transf. **340**, 109432 (2025).
[30]E. Xu and J. Tennyson, "Empirical rovibrational energy levels for carbonyl sulphide," Molecular Physics **122**, e2279694 (2024).
[31]E. O. Dobrolyubov, I. V. Polyakov, D. V. Millionshchikov, and S. V. Krasnoshchekov, "Vibrational resonance phenomena of the OCS isotopologues studied by resummation of high-order Rayleigh–Schrödinger perturbation theory," Journal of Quantitative Spectroscopy and Radiative Transfer **316**, 108909 (2024).
[32]A. Owens, "A highly accurate potential energy surface for carbonyl sulphide (OCS): how important are the ab initio calculations?" Phys. Chem. Chem. Phys. **26**, 17684–17694 (2024).
[33]A. Owens, S. N. Yurchenko, and J. Tennyson, "Exomol line lists–lviii. high-temperature molecular line list of carbonyl sulphide (OCS)," Monthly Notices of the Royal Astronomical Society **530**, 4004–4015 (2024).
[34]X. Huang, I. E. Gordon, T. Bertin, D. W. Schwenke, and T. J. Lee, "Accurate potential energy surface, dipole moment surface, and ir line lists for OCS isotopologues up to 2000 K," Journal of Quantitative Spectroscopy and Radiative Transfer , 109425 (2025).
[35]F. Iachello, *Lie Algebras and Applications (Lecture Notes in Physics)*, Vol. 891 (Springer, Berlin, 2015).
[36]F. Iachello, "Algebraic methods for molecular rotation-vibration spectra," Chemical Physics Letters **78**, 581–585 (1981).
[37]F. Iachello and R. D. Levine, *Algebraic Theory of Molecules* (Oxford University Press, Oxford, 1995).
[38]A. Frank and P. V. Isacker, *Algebraic Methods in Molecular and Nuclear Structure Physics* (John Wiley and Sons, New York, 1994).
[39]S. Oss, "Algebraic models in molecular spectroscopy," in *Adv. Chem. Phys.* (John Wiley & Sons, Ltd, 1996) pp. 455–649.
[40]F. Iachello and S. Oss, "Algebraic approach to molecular spectra: Two-dimensional problems," The Journal of chemical physics **104**, 6956–6963 (1996).
[41]F. Pérez-Bernal and F. Iachello, "Algebraic approach to two-dimensional systems: Shape phase transitions, monodromy, and thermodynamic quantities," Physical Review A—Atomic, Molecular, and Optical Physics **77**, 032115 (2008).
[42]F. Iachello, F. Pérez-Bernal, and P. Vaccaro, "A novel algebraic scheme for describing nonrigid molecules," Chemical Physics Letters **375**, 309–20 (2003).
[43]F. Pérez-Bernal, L. F. Santos, P. H. Vaccaro, and F. Iachello, "Spectroscopic signatures of nonrigidity: Algebraic analyses of infrared and Raman transitions in nonrigid species," Chem. Phys. Lett. **414**, 398 – 404 (2005).
[44]R. N. Dixon, "Higher Vibrational Levels of a Bent Triatomic Molecule," Trans. Faraday Soc. **60**, 1363–1368 (1964).
[45]K. Yamada and M. Winnewisser, "A Parameter to Quantify Molecular Quasilinearity," Z. Naturforsch. A **31**, 139 – 144 (1976).
[46]M. S. Child, "Quantum states in a champagne bottle," J. Phys. A: Math. and General **31**, 657–670 (1998).
[47]M. S. Child, T. Weston, and J. Tennyson, "Quantum monodromy in the spectrum of H_2O and other systems: New insight into the level structure of quasi-linear molecules," Mol. Phys. **96**, 371–379 (1999).
[48]M. A. Caprio, P. Cejnar, and F. Iachello, "Excited state quantum phase transitions in many-body systems," Annals of Physics **323**, 1106 – 1135 (2008).
[49]P. Cejnar and P. Stransky, "Impact of quantum phase transitions on excited-level dynamics," Phys. Rev. E **78** (2008).
[50]P. Cejnar, P. Stránský, M. Macek, and M. Kloc, "Excited-state quantum phase transitions," Journal of Physics A: Mathematical and Theoretical **54**, 133001 (2021).
[51]D. Larese and F. Iachello, "A study of quantum phase transitions and quantum monodromy in the bending motion of non-rigid molecules," J. Mol. Struct. **1006**, 611–28 (2011).
[52]D. Larese, F. Pérez-Bernal, and F. Iachello, "Signatures of quantum phase transitions and excited state quantum phase transitions in the vibrational bending dynamics of triatomic molecules," Journal of Molecular Structure **1051**, 310–327 (2013).
[53]J. Khalouf-Rivera, F. Pérez-Bernal, and M. Carvajal, "Excited state quantum phase transitions in the bending spectra of molecules," Journal of Quantitative Spectroscopy and Radiative Transfer **261**, 107436 (2021).
[54]J. Khalouf-Rivera, M. Carvajal, and F. Pérez-Bernal, "Quantum fidelity susceptibility in excited state quantum phase transitions: Application to the bending spectra of nonrigid molecules," SciPost Phys. **12**, 002 (2022).
[55]J. Khalouf-Rivera, F. Pérez-Bernal, and M. Carvajal, "Anharmonicity-induced excited-state quantum phase transition in the symmetric phase of the two-dimensional limit of the vibron model," Phys. Rev. A **105**, 032215 (2022).
[56]J. Novotný and P. Stránský, "Relative asymptotic oscillations of the out-of-time-ordered correlator as a quantum chaos indicator," Phys. Rev. E **107**, 054220 (2023).
[57]M. Sánchez-Castellanos, R. Lemus, M. Carvajal, and F. Pérez-Bernal, "The potential energy surface of CO_2 from an algebraic approach," International Journal of Quantum Chemistry **112**, 3498–3507 (2012).
[58]M. Sánchez-Castellanos, R. Lemus, M. Carvajal, F. Pérez-Bernal, and J. Fernández, "A study of the Raman spectrum of CO_2 using an algebraic approach," Chemical Physics Letters **554**, 208–213 (2012).
[59]M. M. Estévez-Fregoso and R. Lemus, "Connection between the su(3) algebraic and configuration spaces: bending modes of linear molecules," Molecular Physics **116**, 2374–2395 (2018).
[60]M. Bermúdez-Montaña, M. Rodríguez-Arcos, M. Carvajal, C. Ostertag-Henning, and R. Lemus, "Algebraic vibrational description of the symmetric isotopologues of CO_2: $^{13}C^{16}O_2$, $^{12}C^{18}O_2$ and $^{12}C^{17}O_2$," Chemical Physics **557**, 111481 (2022).
[61]M. Bermúdez-Montaña, M. Rodríguez-Arcos, M. Carvajal, C. Ostertag-Henning, and R. Lemus, "A spectroscopic description of asymmetric isotopologues of CO_2," The Journal of Physical Chemistry A **127**, 6357–6376 (2023).
[62]E. Suárez, O. Guzmán-Juárez, and R. Lemus, "A general local algebraic approach for molecules with normal mode behavior: Application to FCN," Computational and Theoretical Chemistry **1244**, 115069 (2024).
[63]R. Lemus, M. Sánchez-Castellanos, F. Pérez-Bernal, J. M. Fernández, and M. Carvajal, "Simulation of the Raman Spectra of CO_2: Bridging the Gap Between Algebraic Models and Experimental Spectra," J. Chem. Phys. **141**, 054–306 (2014).
[64]M. Bermúdez-Montaña, M. Carvajal, F. Pérez-Bernal, and R. Lemus, "An Algebraic Alternative for the Accurate Simulation of CO_2 Raman Spectra," J. Raman Spectrosc. **51**, 569–583 (2020).
[65]L. F. Santos and F. Pérez-Bernal, "Structure of eigenstates and quench dynamics at an excited-state quantum phase transition," Phys. Rev. A **92**, 050101 (2015).
[66]L. F. Santos, M. Távora, and F. Pérez-Bernal, "Excited-state quantum phase transitions in many-body systems with infinite-range interaction: Localization, dynamics, and bifurcation," Phys. Rev. A **94**, 012113 (2016).
[67]F. Pérez-Bernal and O. Álvarez-Bajo, "Anharmonicity effects in the bosonic u(2)-so(3) excited-state quantum phase transition," Phys. Rev. A **81**, 050101 (2010).
[68]M. Newville, T. Stensitzki, D. B. Allen, M. Rawlik, A. Ingargiola, and A. Nelson, "LMFIT: non-linear least-square minimization and curve-fitting for Python," Astrophysics Source Code Library , ascl–1606 (2016).
[69]V. Zelevinsky, B. Brown, N. Frazier, and M. Horoi, "The nuclear shell model as a testing ground for many-body quantum chaos," Physics Reports **276**, 85–176 (1996).